# Surface barrier dominated transport in $NbSe_2$

Y. Paltiel, D. T. Fuchs, E. Zeldov, Y. N. Myasoedov, and H. Shtrikman
*Department of Condensed Matter Physics, The Weizmann Institute of Science, Rehovot 76100, Israel*

M. L. Rappaport
*Physics Services, The Weizmann Institute of Science, Rehovot 76100, Israel*

E. Y. Andrei
*Department of Physics and Astronomy, Rutgers University, Piscataway, New Jersey 08855*

(Received 3 August 1998)

Transport current distribution in clean 2H-$NbSe_2$ crystals is studied by measuring the self-induced magnetic field across the sample. Below $T_c$ most of the current flows at the edges of the crystals due to strong surface barriers, which are found to dominate the transport properties and the resistive transition. The measured critical current is determined by the critical current for vortex penetration through the surface barrier rather than by bulk pinning. [S0163-1829(98)51446-4]

Vortices in type-II superconductors have to overcome surface and geometrical barriers (SB) in order to exit or penetrate into the superconductor. The effect of SB on the magnetic properties has been extensively studied theoretically.[1–4] In recent years numerous studies have shown that SB dominate the magnetization behavior in clean crystals of high-temperature superconductor (HTSC), in particular at elevated temperatures.[5–10] Since bulk pinning is strongly reduced by thermal fluctuations, the relative importance of the SB is expected to grow with temperature.[11] At low temperatures, in contrast, and in low-$T_c$ superconductors in general, bulk pinning is expected to be the main source of hysteretic magnetization. Recent theoretical works[12,13] have suggested that SB can also significantly modify the transport properties of superconductors. Current distribution measurements in $Bi_2Sr_2CaCu_20_8$ (BSCCO) crystals[14,15] have revealed that over a wide range of temperatures and fields, the transport current indeed flows predominantly at the edges of the crystals where vortices enter and exit the superconductor. In this paper we report that SB dominate the transport behavior also in the low-$T_c$ superconductor $NbSe_2$. SB should therefore be of significant importance in a wide range of superconductors in affecting the transport as well as the magnetic properties. Since SB compete with bulk pinning in determining the dynamics of vortices, SB may become the dominant mechanism in materials with low bulk pinning.

High-purity 2H-$NbSe_2$ crystals with $T_c = 7.2$ K were grown as described previously.[16] Several crystals were cleaved and cut into a rectangular strip shape. The data presented here are for one of the crystals with dimensions of $1.46\ \text{mm}(l) \times 0.35\ \text{mm}(w) \times 0.04\ \text{mm}(d)$. The features reported below were observed in all the investigated crystals. Four pads for electrical contacts of $0.1 \times 0.1\ \text{mm}^2$ with 0.13 mm separation between pairs were prepared by Ag/Au evaporation. The crystal was mounted onto an array of 19 two-dimensional electron gas GaAs/AlGaAs Hall sensors $10 \times 10\ \mu\text{m}^2$ each with a 10 $\mu$m separation. The inset to Fig. 1 shows a schematic top view of the experimental setup. A dc magnetic field $H_{dc}$ was applied perpendicular to the plane of the sensors and parallel to the $c$ axis of the crystal. An ac transport current $I_{ac}$ in the range of 1–30 mA at 65 Hz was applied, and the corresponding self-induced magnetic field $B_{ac}(x)$ across the crystal was measured by the Hall sensor array. The four-probe resistance of the sample was measured under the same conditions using a lock-in amplifier.

There are three main regimes for the flow of the transport

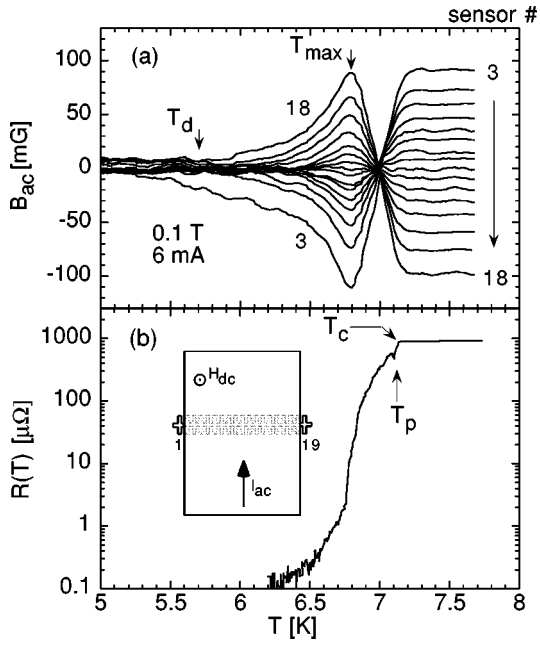


FIG. 1. (a) Transport current self-induced field $B_{ac}$ as measured by sensors 3 to 18 across the width of a $NbSe_2$ crystal at $H_{dc} = 0.1$ T and $I_{ac} = 6$ mA. At the crossing point of the curves half of the transport current flows in the bulk and half at the sample edges. At lower temperatures the inverted curves indicate that most of the current flows at the edges. Vortices are immobile below $T_d$. (b) Corresponding four-probe resistance measurement. The resistance drops sharply at $T_{max}$ and shows a tail at lower temperature due to weak flux creep. Inset: schematic cross section of the sample mounted on an array of 19 Hall sensors.

 

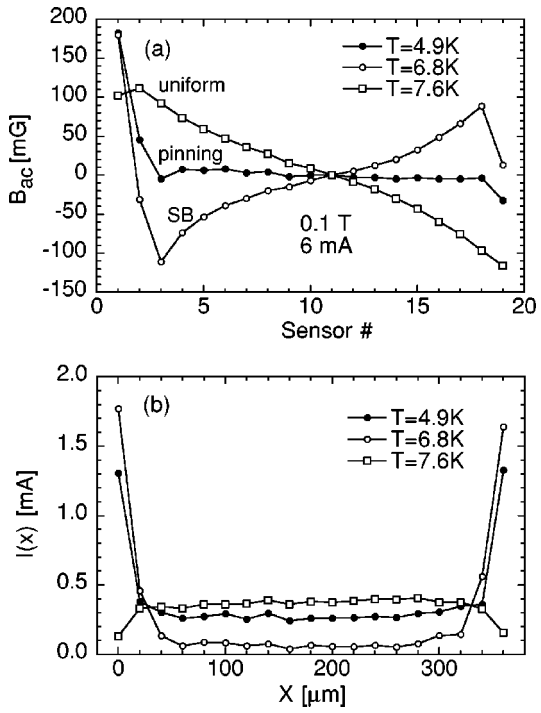


FIG. 2. (a) Three $B_{ac}(x)$ profiles at different temperatures taken from Fig. 1(a). (b) Transport current distributions obtained by inversion of $B_{ac}$ in (a). Above $T_c$ the current flows uniformly across the crystal (7.6 K profile). At $T=T_{max}=6.8$ K practically all the current flows at the two edges of the sample due to strong SB. At low temperatures the vortices are immobile and the current is distributed in the corresponding self-shielding form (4.9 K profile).

current as described in Ref. 14: (a) Uniform current flow in the bulk of the sample. In this case, applying the Biot-Savart law, the perpendicular component of the self-induced field, as measured by the sensors, decreases monotonically from the left edge to the right. (b) Surface barrier dominated flow for which most of the current flows at the two edges of the crystal in order to drive the vortices over the entry and exit SB. The resulting self-induced field across the crystal is opposite in sign and increases from left to right. (c) Vortex pinning which prevents vortex motion and results in zero self-field inside the sample. The corresponding transport current, in this case, has a characteristic Meissner distribution with a reduced current in the center and enhanced at the edges.[17–19]

Figure 1(a) shows an example of the self-induced field $B_{ac}$ as a function of temperature at $H_{dc}=0.1$ T and $I_{ac}=6$ mA. For clarity, only the sensors 3 to 18, which are under the crystal, are shown. The corresponding resistance is shown in Fig. 1(b). The observed behavior is very similar to that reported for BSCCO crystals.[14] Above $T_c$, the current flows uniformly as expected, and $B_{ac}$ decreases monotonically from the left edge of the crystal (sensor 3) to the right edge (sensor 18). This behavior is seen more clearly in Fig. 2(a), which shows $B_{ac}(x)$ profile for all the sensors at 7.6 K. As the temperature is decreased, the SB sets in immediately below $T_c$ drawing an increasingly larger fraction of the current to the edges. This gives rise to the observed temperature dependence of $B_{ac}$ in Fig. 1(a): a drop in $B_{ac}$ just below $T_c$, followed by crossing of the curves and sign reversal at lower temperatures. At the crossing point, half of the transport current flows across the bulk and the other half at the two edges of the sample. At $T=T_{max}$ [see Fig. 1(a)] most of the current flows at the crystal edges and the self-field profile inside the crystal is completely inverted relative to the uniform flow case, as shown in Fig. 2(a) for $T=6.8$ K. Note that any bulk mechanism or finite skin depth effect will result in $B_{ac}$ which is either zero (perfect shielding) or positive in the left half of the sample (finite shielding), but it cannot cause $B_{ac}$ to become negative (negative permeability[10]). The sign reversal of $B_{ac}$ is a unique property of the SB. As the temperature is further decreased, the vortices become immobile for $T<T_d$ due to the combination of the SB and bulk pinning, resulting in a vanishing $B_{ac}$ response within the crystal as shown by the 4.9 K profile in Fig. 2(a).

In Ref. 14 arrays of seven Hall sensors were used, which allowed mapping of $B_{ac}$ typically over only half of the sample width. Here we have extended the arrays to 19 sensors that provide more detailed $B_{ac}(x)$ over the entire sample width. This improvement has two significant advantages. First, we can readily examine both edges of the sample and evaluate the symmetry of the current distribution. The second major advantage is that having 19 values of $B_{ac}$ field across the sample is sufficient in order to directly invert the field distribution into the current distribution. We represent the sample by 19 current filaments located at about half of the crystal thickness and equally spaced across the width. The currents in the filaments are obtained by inverting the $19\times19$ matrix that transforms between the current and the field values using the Biot-Savart law. Figure 2(b) shows the obtained $I(x)$ corresponding to the three field profiles in Fig. 2(a). As expected, above $T_c$ the current flows uniformly across the crystal (7.6 K profile). However, below $T_c$ the current starts to accumulate at the edges due to the strong SB. At $T=T_{max}$ practically all the current flows at the two edges in a form of two $\delta$ functions with negligible current in the bulk (6.8 K profile). At low temperatures, 4.9 K profile, the vortices become immobile and the current is distributed in the corresponding self-shielding form[17–19] with a minimum in the center and a rapid increase near the edges. Note that the actual current distribution is continuous across the width and the thickness of the crystal, and hence our derivation of the discreet current filaments in Fig. 2(b) is only an approximation. Yet, this simple analysis clearly visualizes the underlying mechanisms, and in particular the main transition from a uniform current flow above $T_c$ to SB dominated flow below $T_c$. This finding shows that in clean $NbSe_2$ crystals the vortex flow rate is determined by the transmission probability through the SB rather than by bulk vortex dynamics. An important experimental implication is that the transport measurements in this case reflect the resistive properties of the SB rather than the bulk properties.

Another aspect of the SB is its asymmetry with respect to vortex entry and exit.[1] Vortex entry requires a larger force than vortex exit. As a result a larger current flows at the vortex entry edge in order to maintain the same vortex flow rate throughout the sample. The role of the edges is interchanged as the direction of the ac current changes, with a larger current flowing on the opposite edge of the crystal. This mechanism results in a significant local second harmonic self-field signal, as shown in Fig. 3 for $H_{dc}=0.5$ T and $I_{ac}=6$ mA. Second harmonic is a unique feature of the

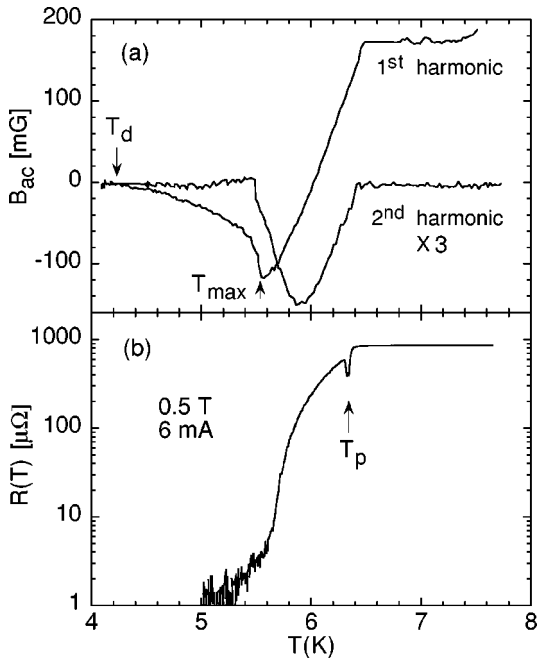


FIG. 3. First and second (multiplied by 3) harmonics of $B_{ac}$ as measured by sensor 3 (a), and the corresponding resistance (b) at $H_{dc}=0.5$ T and $I_{ac}=6$ mA. The SB, and hence the second-harmonic signal, set in immediately below $T_c$. At $T_{max}$, $I_{ac}=I_c^b+I_c^s$ and $B_{ac}$, the second-harmonic signal, and the resistance drop sharply. The narrow dip in the resistance at $T_p$ is the peak effect in $NbSe_2$.

SB due to its asymmetry with respect to the current direction. Bulk vortex dynamics, in contrast, results only in odd harmonics, since bulk $I$-$V$ characteristics are antisymmetric with respect to the current. Figure 3 shows that the second harmonic signal, and hence the SB, set in immediately below $T_c$ concurrently with the resistive drop. The narrow dip in the resistance at $T_p$ in Fig. 3 is the common peak effect in $NbSe_2$,[20–23] which in our high-purity crystals is extremely narrow [see also Fig. 1(a)]. Within our experimental resolution we do not observe substantial changes in current distribution in this narrow peak-effect region.

In contrast to BSCCO, the thermal activation of vortices in $NbSe_2$ is weak due to much lower $T_c$ and lower anisotropy. We can therefore simplify the description by analyzing the behavior in Fig. 3 in terms of bulk and surface barrier critical currents, $I_c^b$ and $I_c^s$, respectively. Let us first consider the case of finite bulk pinning with no SB, namely $I_c^s=0$. The bulk critical current $I_c^b$ is generally expected to increase with decreasing temperature, but as long as the applied current is larger than $I_c^b(T)$, the current should flow uniformly across the sample.[17–19] As a result, $B_{ac}$ should be positive like above $T_c$, and there should be no second-harmonic signal. When $I_c^b(T)$ approaches the value of the applied current at some characteristic temperature $T_{max}$, vortices stop moving, and $B_{ac}$ should drop rapidly from the full positive value to zero as the temperature is further decreased. This scenario is inconsistent with the data in Fig. 3(a): $B_{ac}$ is negative instead of positive above $T_{max}$, and in addition, significant second harmonic is present. Furthermore, below $T_{max}$, $B_{ac}$ does drop rapidly, but this drop occurs while $B_{ac}$ is negative rather than positive.

We now consider the opposite scenario of finite SB with no bulk pinning, $I_c^b=0$. Since $I_c^s(T)$ is related to the critical field $H_c(T)$, it is expected to grow linearly below $T_c$. Therefore, upon cooling, a progressively larger fraction of the applied current should be drawn towards the edges. The corresponding $B_{ac}$ should drop approximately linearly from a full positive value at $T_c$ down to a full negative value at a characteristic temperature at which $I_c^s(T)$ reaches $I_{ac}$, and as a result practically all the applied current flows at the edges. In this temperature interval a significant second-harmonic signal should be also present, as explained above. The corresponding resistivity of the sample should decrease gradually below $T_c$ with a sharp drop towards zero at the same characteristic temperature. The data in Fig. 3 above $T_{max}$ are fully consistent with this scenario, thus allowing us to identify $T_{max}$ as the characteristic temperature at which $I_{ac}=I_c^s(T)$.

Now let us examine the behavior below $T_{max}$ where $I_{ac}<I_c^s(T)$ and no vortices can exit or penetrate into the sample (in absence of thermal activation). Yet, if $I_c^b=0$ the vortices can move freely *inside* the sample and change their distribution according to $B_{ac}$ imposed by the full $I_{ac}$ flowing on the edges. Since the edges have already absorbed all of $I_{ac}$, there should be no further change in the current distribution below $T_{max}$, and $B_{ac}$ should remain constant at its full negative value [as observed in BSCCO (Ref. 14)]. On the other hand, if a small bulk $I_c^b$ is present in addition to $I_c^s$, $B_{ac}$ should drop sharply to zero below $T_{max}$ since vortices become immobile. $T_{max}$ in this case corresponds to the temperature at which $I_{ac}$ becomes equal to the total critical current $I_c(T)=I_c^b+I_c^s$. The pronounced drop of $B_{ac}$ at $T_{max}$ in Fig. 3(a) indicates therefore the existence of some finite bulk $I_c^b$. The fact that $B_{ac}$ is practically fully inverted at $T_{max}$ shows, however, that $I_c^b \ll I_c^s$. Note also that the second-harmonic signal should be absent below $T_{max}$, since no vortices penetrate through the SB, consistent with the data in Fig. 3(a). $B_{ac}$ instead of remaining constant, shows a rapid decay below $T_{max}$. The tail of $B_{ac}$ as well as the weak resistive tail below $T_{max}$ indicate, furthermore, that a small flux creep is present resulting in some finite vortex motion. Note, that even in this weak creep regime $B_{ac}$ is inverted, showing that most of the current flows at the edges and vortex dynamics is governed by SB. The vortices become fully immobile only at a lower temperature $T_d$, below which the creep stops within our resolution.

Finally, we demonstrate here that the above condition, that the total critical current $I_c$ is determined mainly by the critical current of the SB, holds over the entire investigated range of temperatures and fields. At low temperatures and relatively low current, the vortices are immobile and the current flows with the characteristic Meissner distribution resulting in vanishing $B_{ac}$. In this case one concludes that the applied current $I_{ac}$ is below the total critical current $I_c=I_c^b+I_c^s$, but the values of the individual critical currents cannot be determined. In order to gain this important information one has to increase the applied current just slightly above the total critical current. In this situation the applied current is precisely divided between the bulk and the edges according to $I_c^b$ and $I_c^s$. As a result the vortices are set in motion, and the corresponding $B_{ac}$ signal provides the information on the

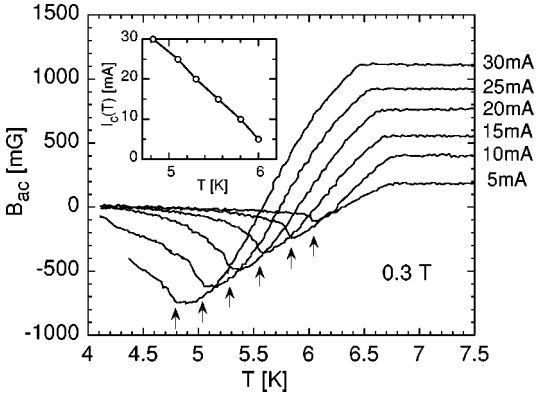


FIG. 4. $B_{ac}$ as measured by sensor 3 for various $I_{ac}$ between 5 and 30 mA at $H_{dc}=0.3$ T. As the current is increased vortices become mobile at progressively lower temperatures. The arrows indicate the temperatures at which the corresponding $I_{ac}$ equals $I_c(T)$. The negative $B_{ac}$ values at these temperatures show that $I_c^b \ll I_c^s$. Inset: temperature dependence of the total critical current $I_c$ at $H_{dc}=0.3$ T.

relative importance of $I_c^b$ and $I_c^s$. Such a measurement is presented in Fig. 4 which shows $B_{ac}$, as measured by sensor 3, at various $I_{ac}$ between 5 and 30 mA at 0.3 T. The arrows indicate the temperatures $T_{max}$ at which $I_{ac}=I_c(T)=I_c^b+I_c^s$ for the various applied currents as described above. The corresponding $I_c(T)$ dependence is shown in the inset. We find that in all cases when $I_{ac}$ reaches $I_c(T)$ the corresponding $B_{ac}$ signal is fully inverted [as the 6.8 K profile in Fig. 2(a)] indicating that practically all the current flows at the edges, and that $I_c^b \ll I_c^s$. Thus, in clean crystals of $NbSe_2$ the measured $I_c$ reflects mainly the critical current of the SB and not the bulk critical current.

In summary, the distribution of transport current in clean platelet crystals of 2H-$NbSe_2$ was studied by measuring the self-induced magnetic field. The use of extended arrays of Hall sensors allows for a direct inversion of the self-field profile into the current distribution profile across the crystal width. Below $T_c$ the current is found to flow predominantly at the sample edges due to strong surface barriers. The SB govern the apparent resistivity of the crystals. Furthermore, the measured critical current is determined by the critical current of the SB barrier rather than by bulk critical current.

We are grateful to A. Wold for the high purity $NbSe_2$ crystals, and to G. Jung and S. Bhattacharya for helpful discussions. This work was supported by Grant No. 97-00424 from the United States-Israel Binational Science Foundation (BSF), Jerusalem, Israel, by the MINERVA Foundation, Munich, Germany, and by the Philip M. Klutznick Fund for Research.

[1] C. P. Bean and J. D. Livingston, Phys. Rev. Lett. **12**, 14 (1964).
[2] J. R. Clem, in *Low Temperature Physics—LT 13*, edited by K. D. Timerhaus, W. J. O'Sullivan, and E. F. Hammel (Plenum, New York, 1974), Vol. 3, p. 102.
[3] L. Burlachkov, Phys. Rev. B **47**, 8056 (1993).
[4] E. Zeldov *et al.*, Phys. Rev. Lett. **73**, 1428 (1994).
[5] N. Chikumoto, M. Konczykowski, N. Motohira, and A. P. Malozemoff, Phys. Rev. Lett. **69**, 1260 (1992).
[6] M. Konczykowski, L. I. Burlachkov, Y. Yeshurun, and F. Holtzberg, Phys. Rev. B **43**, 13 707 (1991).
[7] M. V. Indenbom *et al.*, Physica C **235–240**, 201 (1994).
[8] C. J. van der Beek, M. V. Indenbom, G. D'Anna, and W. Benoit, Physica C **258**, 105 (1996).
[9] E. Zeldov *et al.*, Europhys. Lett. **30**, 367 (1995).
[10] N. Morozov *et al.*, Phys. Rev. Lett. **76**, 138 (1996).
[11] L. Burlachkov and V. M. Vinokur, Physica C **235–240**, 2993 (1994).
[12] L. Burlachkov, A. E. Koshelev, and V. M. Vinokur, Phys. Rev. B **54**, 6750 (1996).
[13] M. Benkraouda and J. R. Clem (unpublished).
[14] D. T. Fuchs *et al.*, Nature (London) **391**, 373 (1998).
[15] D. T. Fuchs *et al.*, Phys. Rev. Lett. **80**, 4971 (1998).
[16] H. N. S. Lee, H. McKinzie, D. S. Tannhauser, and A. Wold, J. Appl. Phys. **40**, 602 (1969).
[17] E. Zeldov, J. R. Clem, M. McElfresh, and M. Darwin, Phys. Rev. B **49**, 9802 (1994).
[18] E. H. Brandt and M. V. Indenbom, Phys. Rev. B **48**, 12 893 (1993).
[19] W. T. Norris, J. Phys. D **3**, 489 (1970).
[20] S. Bhattacharya and M. J. Higgins, Phys. Rev. Lett. **70**, 2617 (1993); Phys. Rev. B **49**, 10 005 (1994).
[21] W. Henderson *et al.*, Phys. Rev. Lett. **77**, 2077 (1996).
[22] K. Ghosh *et al.*, Phys. Rev. Lett. **76**, 4600 (1996).
[23] G. D'Anna *et al.*, Phys. Rev. B **54**, 6583 (1996).